Department of Physics and Astronomy
University of Heidelberg

Bachelor Thesis in Physics
submitted by

Alexander Junkermann

born in Worms (Germany)

2020

Detector Parametrisation Studies of the Mu3e Tile Detector

This Bachelor Thesis has been carried out by Alexander Junkermann at the
Kirchhoff Institute for Physics in Heidelberg
under the supervision of
Prof. Dr. Hans-Christian Schultz-Coulon

Kurzfassung

Mit dem Mu3e Experiment wird nach dem Lepton-Flavour verletzenden Zerfall $\mu^+ \to e^+e^+e^-$ gesucht. Eine Entdeckung wäre ein direkter Hinweis auf eine Physik jenseits des Standardmodells. Bei sehr hohen Myonen-Zerfallraten soll eine Sensitivität von 10^{-16} erzielt werden. Zur Messung werden sehr präzise Detektoren benötigt. Der Tile Detektor des Experiments ist für die präzise Zeitmessung verantwortlich und wird dafür genutzt, um Untergrund-Ereignisse zu unterdrücken.
Im Rahmen dieser Arbeit wird untersucht, wie die Totzeit einzelner Kanäle des Tile Detekors im Zusammenhang mit der deponierten Energie der Teilchen und zugehöriger Trigger steht, um eine ausreichende Detektionsrate zu garantieren. Es wurden bisher Totzeiten um 260 ns [1] erwartet. Die Werte, die aufgrund der Messungen dieser Arbeit für die momentanen Einstellungen des Tile Detectors für das Experiment erwartet werden, liegen bei einer Biasspannung von 57.5 V eine Größenordnung höher mit bis zu (1.8 ± 0.22)µs. Dies würde einem Signalverlust von bis zu $(10.2 \pm 1.1)\%$ entsprechen. Bei einer Biasspannung von 54 V hingegen wird eine Totzeit von bis zu (0.59 ± 0.06)µs und einem entsprechend Signalverlust von bis zu $(3.5 \pm 0.3)\%$ erwartet. Diese Ergebnisse stellen einen signifikanten Einfluss auf die Detektionsrate dar. Daher sollte die Totzeit bei zukünftigen Messungen mitbeachtet werden, sodass eine hohe Detektionsrate garantiert bleibt.

Abstract

The Mu3e experiment is looking for the Lepton-Flavour violating decay $\mu^+ \to e^+e^+e^-$. A discovery would be an indication for physics beyond the Standard Model. While high muon decay rates are achieved, the aim is a high sensitivity of 10^{-16} to suppress background events. This requires extremely precise detectors. The Tile Detector is responsible for achieving a high time resolution.
In the scope of this work, the relation of the Tile Detectors single channels deadtimes to the energy deposited by a particle in the detector is investigated. This knowledge is needed to guarantee a sufficient detection rate. Previously deadtimes of around 260 ns [1] were expected. The measurements conducted for this thesis propose for the former chosen settings at a bias voltage of 57.5 V deadtimes of up to (1.8 ± 0.22)µs. This would correspond to a signal loss of up to $(10.2 \pm 1.1)\%$. A lower bias voltage of 54 V would correspond only to a deadtime of (0.59 ± 0.06)µs which would correspond to a signal loss of up to $(3.5 \pm 0.3)\%$. Those values show a significant change for the detection rate of the Mu3e experiment, which underlines the importance of deadtime optimisation for the next testbeam trials in order to maintain a high detection rate.

Contents

1 Introduction **2**
1.1 Motivation . . . 2
1.2 Design of the Mu3e Experiment . . . 2

2 The Tile Detector **4**
2.1 Tile Detector Structure . . . 4
2.2 Silicon Photomultipliers . . . 5
2.2.1 Geiger-Mode Avalanche Photodiode . . . 5
2.2.2 Silicon Photomultiplier . . . 6
2.3 MuTRiG . . . 8

3 Characterisation Measurements **10**
3.1 The Na-22 Spectrum . . . 10
3.1.1 Compton Scattering and the Compton Edge . . . 11
3.1.2 The Na-22 Spectrum . . . 12
3.2 Measurement Setup . . . 13
3.2.1 Deadtime Measurements . . . 14
3.2.2 Signal Height Measurements . . . 15
3.2.3 Calibration Measurements . . . 15

4 Results **16**
4.1 Deadtime Measurements . . . 16
4.2 Signal Height Measurements . . . 18
4.3 Calibration Measurements . . . 20
4.4 Combined Results of the Measurements . . . 21
4.5 Estimations for the Mu3e Experiment . . . 24
4.6 Discussion and Limits of the Method and the Predictions . . . 28

5 Summary **29**

A Images of the Electronics **31**
A.1 Setup 1 . . . 32
A.2 Setup 2 . . . 33

1 Introduction

1.1 Motivation

In 2012, in a letter of intent [2], an experiment has been proposed to search for the lepton flavour violating decay $\mu^+ \rightarrow e^+e^+e^-$ at the Paul Scherrer Institute (PSI) in Switzerland. The experiment is called Mu3e and is designed to be complementary to other experiments researching lepton flavour violating models. It is planned that the PSI will receive an upgrade to its muon beamline, such that it can deliver up to 10^9 muons per second. This upgrade aims to achieve a sensitivity of 10^{-16} for the above-mentioned decay. This will improve the current exclusion limit by four orders of magnitude, which was achieved by the SINDRUM experiment. While the Standard Model including neutrino oscillations predicts a branching ratio of about 10^{-54} for the $\mu^+ \rightarrow e^+e^+e^-$ decay, extending theories beyond the Standard Model suggest an experimentally measurable decay by interactions with unknown particles at loop level.
The properties of the decay are, that the sum of the electron energies should equal the muon mass and the vector sum of all electron momenta should cancel out. Thereby with a high momentum resolution, processes such as $\mu^+ \rightarrow e^+e^+e^-\nu_e\bar{\nu}_\mu$, where the neutrinos carry away some energy, can be suppressed. In addition, high vertex and time resolution are needed to suppress accidental background.

1.2 Design of the Mu3e Experiment

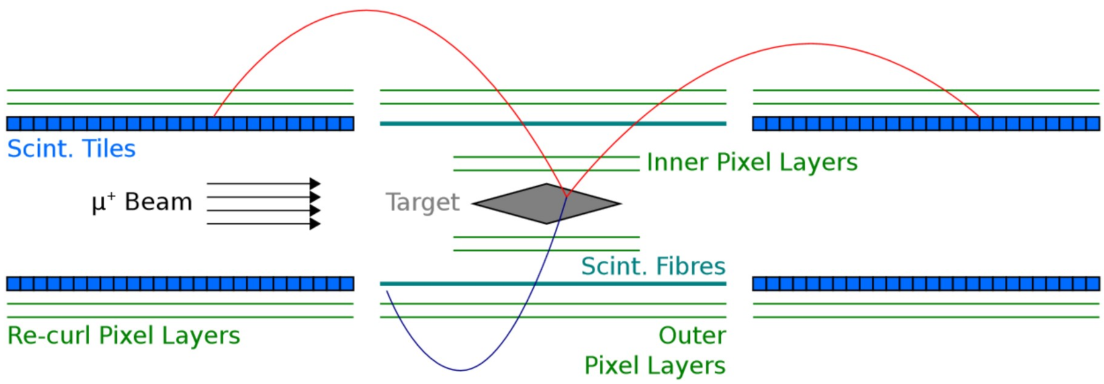

Figure 1: Schematic of the Mu3e Detector Design [1]. The red paths indicate the flight path of positrons and the blue paths correspond to the flight path of electrons.

As seen in Fig. 1, the experimental design is divided into three stations. In the center of the experiment a thin hollow double cone is placed as a target, where the low energetic muons are stopped and will decay. Around the target two layers of pixel detectors are located to determine the particle production vertices. Following the pixel layers there are scintillating fibres for timing resolution and another two pixel layers for resolving the curved flight path of the electrons and positrons. On the upstream and the downstream side of the target are the recurl stations to which the electrons and positrons are directed back by the 1 T magnetic field after leaving the inner station. The recurl stations provide tracking and timing information of the recurling electrons and positrons. The tracking of the recurling electrons and positrons is done by two pixel detector layers of the same kind as in the central station. The curvature of the charged particles in the magnetic field then allows for the determination of their momentum. The timing measurement inside the recurl stations is provided by the tile detector, which is the focus of this work.

2 The Tile Detector

The Tile Detector inside the recurl stations is one of two timing detector systems located in the Mu3e experiment. It detects the recurling electrons and positrons from the muon decay. This work will only deal with the detection of electrons because electrons and positrons have the same detection behaviour except the fact that the positrons annihilate with another electron when they are almost completely stopped and that the positrons flight curves are bend the other way inside a magnetic field.
The Tile Detector requirements aim for a time resolution below 100 ps while about 100% signal efficiency should be maintained. This poses a challenge due to the expected high particle rates of up to 60 kHz per channel. In the following section the structure of this system will be introduced while Section 2.2 and Section 2.3 focus on the relevant detector parts.

2.1 Tile Detector Structure

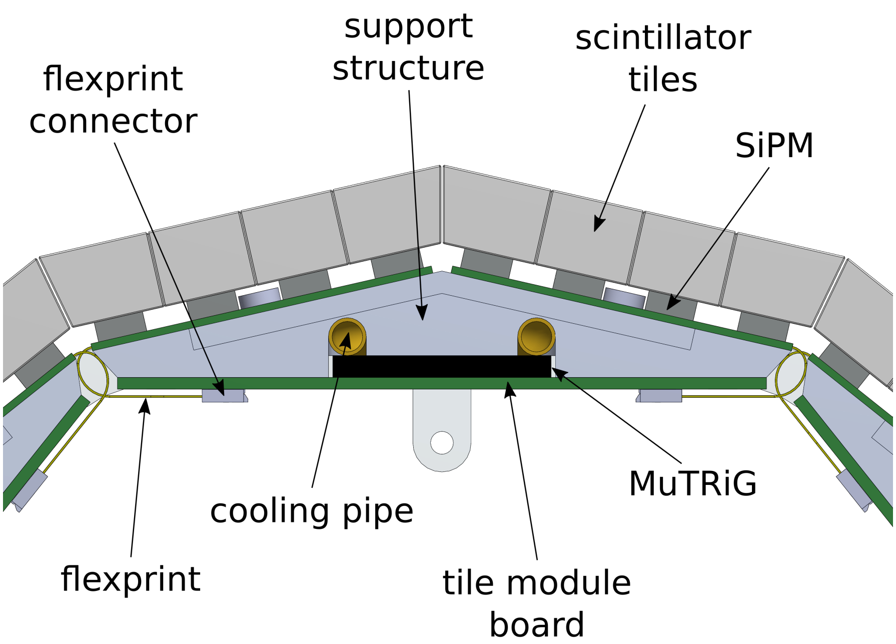

Figure 2: Schematic of the Tile Detector (front view),[H. Klingenmeyer, provided through internal communications].

The Tile Detector consists of the following core components: the scintillating tiles to detect traversing electrons, the Silicon Photomultipliers (SiPM) for scintillating light detection and the MuTRiG chip for the SiPM readout, as well as an aluminium support, a cooling structure and electronic infrastructure. A schematic Fig. 2 of a cutout from the tile detector CAD model shows how the matrices are placed on the structure. One matrix consists of 4x4 scintillating tiles, each with a SiPM underneath. The scintillating tiles are made out of organic scintillator material[1] and are covered on five sides with reflective foil such that the light does not reach other tiles and is directed to the SiPM on the bottom side. The light-detecting SiPMs are soldered on top of a printed circuit board which is attached to the aluminium support. A tile module board assembled on the bottom of the support contains the MuTRiG chip which is connected via a flexprint connector to the SiPMs. The following chapter is supposed to give an introduction about the parts of the tile detector.

2.2 Silicon Photomultipliers

2.2.1 Geiger-Mode Avalanche Photodiode

p-n Junctions The working principle of Geiger-Mode Avalanche Photodiodes (G-APDs) is based on p-n junctions. A p-n junction is an intersection between a positive "p" doped and a negative "n" doped semiconductor material. At the junction, electrons diffuse from the n side to the p side and holes diffuse from the p to the n side. The donor or acceptor atoms can not move while the charge carriers do. This creates on the n side a small positively and on the p side a small negatively charged region. The charged region induces an electric field which counteracts the diffusion process of the charge carriers causing an equilibrium to develop. This area of equilibrium is called depletion region. By applying a so-called reverse bias voltage the depletion region can be enlarged. A larger depletion region is important because due to interactions in the depletion region light detection is possible. This is achieved by applying a positive voltage to the n side and negative voltage to the p side. The required voltage for a large depletion region can be drastically reduced by introducing a layer of intrinsic silicon, resulting in a so-called PIN photodiode (see Fig. 3).

Photon Detection Due to the photoelectric effect, a photon with a sufficient energy hitting the depletion area is able to elevate an electron from the valence band to the conduction band of the material. Thus an electron-hole pair is created. In the electric field, the electron drifts to the n region while the hole drifts to the p region creating a current (see Fig. 3). Because one photon would only correspond to a single electron, an amplification mechanism is needed. This is achieved by introducing a larger doping gradient at the junction, thereby creating a stronger field. If an electron enters the high electric field region it is accelerated and the probability to create more electron-hole pairs by impact ionisation is increased.

[1]Material EJ-228

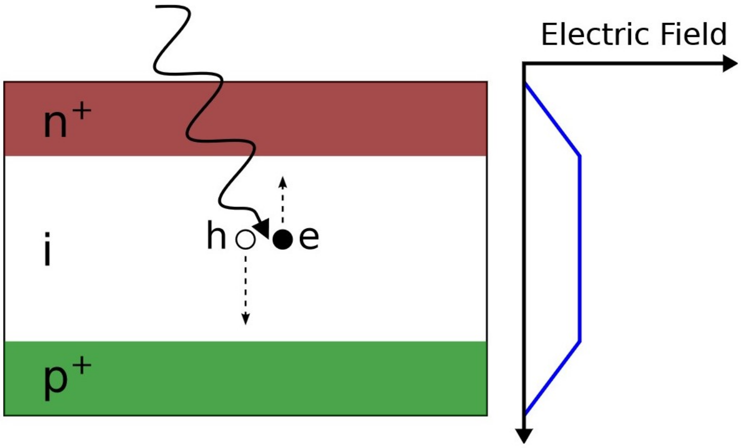

Figure 3: Schematic of a PIN-Diode with an indication of the electric field inside the material and the process of the absorption of a single photon creating an electron(e)-hole(p) pair. The doping of the material is indicated by i, the undoped material, n^+ the strong negative doped material and $p+$ the strong positively doped material. [1]

The created electrons in turn are able to produce more electron-hole pairs resulting in an avalanche mechanism, as indicated in Fig. 4. If the applied bias voltage exceeds a certain level called the breakdown voltage, the electric field reaches a sufficient strength accelerating the holes enough to create new electron-hole pairs. In this so-called Geiger region the avalanche process is self-sustained and during the process a constant current flows, which is called Geiger discharge. This discharge needs to be quenched if new photons are to be detected and not to destroy the device. On the used SiPMs[2] this is achieved passively by connecting the voltage source in series with a quenching resistor to the diode. If the current increases at the resistor, according to Ohm's law there is a voltage drop over the resistor resulting in a decreasing voltage at the diode and eventually stopping the self-sustained avalanche process. The resulting signal has a sharp rise and a slow decrease. The released charge Q during the pulse is nearly a constant value. This is comparable to photo multiplier tubes which have the same working principle except that they tend to be bigger and filled with gas instead of being solid.

2.2.2 Silicon Photomultiplier

A great disadvantage of the G-APD is that it is only able to measure a single photon at a time. This problem is solved by arranging multiple G-APDs in a single sensor called a Silicon Photomultiplier. The SiPM which is used in the tile detector, for example, has 3584 G-APD pixels and a size of 3 mm × 3 mm. The G-APD pixels and their quenching resistors are connected in parallel to the bias voltage as seen in Fig. 5. The output signal is thereby the sum of all the individual

[2]Hamamatsu 13360-3050VE

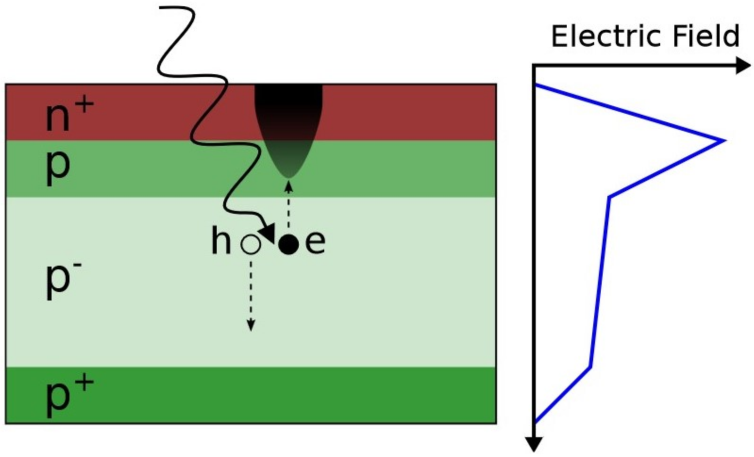

Figure 4: Schematic of a G-APD with with the same indications as in Fig. 3. Additionally p and p^- represent a normal and a weaker positive doped material and an avalanche produced by the electron in the region with the strong field is indicated [1]

circuits with the total charge being the sum of all charges from triggered pixels.

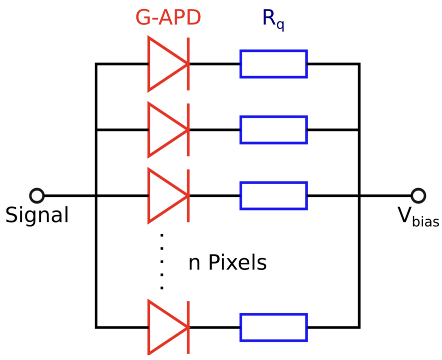

Figure 5: Schematic of the G-APDs with quenching resistors R_q in parallel to form a SiPM [1].

Photon Detection Efficiency The Photon Detection Efficiency (PDE) is one of the most important parameters of a SiPM. It describes the percentage of photons which will be detected by the SiPM. It is given by:

$$\varepsilon_{\mathrm{PDE}}(\lambda, V, T) = (1 - R(\lambda)) \cdot QE(\lambda) \cdot P_{ff} \cdot P_g(\lambda, V, T) \tag{1}$$

The factor $(1 - R(\lambda))$ is the wavelength-dependent probability that a photon is transmitted into the SiPM, while the fill factor P_{ff} gives the percentage of area where an electron-hole pair can be produced. The probability for such an electron-hole pair to be created is given by the energy-dependent Quantum Efficiency $QE(\lambda)$. The last parameter is the Geiger efficiency P_g, describing the chance that an electron-hole pair results in a Geiger discharge. The Geiger efficiency is dependent on the temperature and the voltage of the particle as well as the energy of the incoming photon. The voltage dependency will be used in this thesis in order to emulate different energy levels.

Number of Detected Photons The charge created inside a G-APD during an avalanche process caused by a single photon directly corresponds to the gain of the G-APD. Since all the pixels of the SiPM have approximately the same charge output, the SiPM signal gives information about the number of photons detected. This can be done by measuring the signal amplitudes and thereby obtaining a height distribution. For levels where only a few photons are detected this distribution has distinct peaks whose positions represent the amount of photons detected. Those distributions are called Single Photon Spectra (SPS).

Noise Sources Noise, relevant for SiPMs has three major sources and is introduced in this paragraph to give a basis to discuss the measurements. The first type of source is the Dark Count Rate (DCR) where electron-hole pairs are spontaneously created by either thermal excitation or tunneling. The second source is Cross-Talk (CT) where optical photons which are created during an avalanche in a pixel traverse to the next pixel and trigger a new avalanche. The last source of noise are the so-called afterpulses in which energy from an avalanche is delayed or stored in the materials lattice and released after a period of time, thus creating a new avalanche.

2.3 MuTRiG

The Muon Timing Resolver including Gigabit-link (MuTRiG) [3] chip is an application-specific integrated circuit and was developed for the timing detectors of the Mu3e experiment. It is the successor of the STiCv3 [1] chip and has been adapted to fulfil requirements of the Tile Detector: a timing resolution better than 100 ps at close to 100% efficiency as well as hit rates of up to 60 kHz per channel. The timing measurement in the MuTRiG is done by using a leading edge discrimination method. It checks whether the signal is above an adjustable threshold and for the time it is above the threshold, a constant signal is passed. In the case of the MuTRiG, two discrimination signals are used, as shown in Fig. 6. The one with the lower threshold is called T-Trigger while the one with the higher threshold is the so-called E-Trigger. Those two signals are combined and a XOR Output is generated (see Fig. 6 for principle of signal processing). The first rising edge of the XOR signal contains the timing information while from the difference between first and second rising edge, the energy information can be obtained. The rising edges are read out by a Time-to-Digital Converter (TDC). However, the channel is occupied until the second falling edge of the XOR output. This length of this so-called deadtime, can render the detector inefficient. The investigation of the deadtime, which is the main focus of this work, is therefore of great importance. The focus will be on measuring the energy dependence of the deadtime.

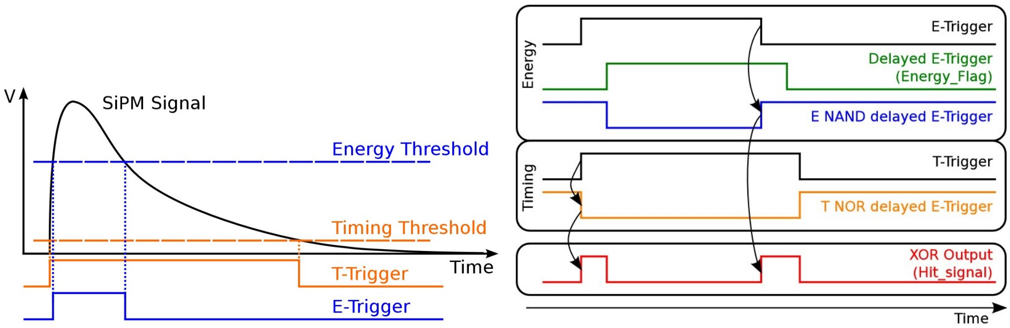

Figure 6: Schematic of the MuTRiG trigger principle [3]. The figure on the left hand side shows how the analogue SiPM signal is converted to a rectangular shape, while the right hand side shows how it is processed. The black arrows show how the signal is passed through the parts. The E-Trigger is processed with a delay because otherwise the rising edge in the final signal would be to small for the time to digital converter to be detected.

3 Characterisation Measurements

In order to quantify the relation between the deadtime and the energy deposited by detected particles, a way of measuring both is needed. The usual approach would be to take a suitable measurement setup to a particle accelerator, which provides electrons with a well known calibrated energy. Unfortunately, this was not possible due to restrictions because of the COVID-19 pandemic. Furthermore, a γ source with known energies could not be used since the scintillators used for the Tile Detector are too thin for high-energetic photon detection. Another method would be to use a pulsed light source to illuminate the detector SiPMs directly. The amount of photons could then be referenced to an energy. This method was deemed unsuitable because the laser pulse distribution would have been too far from the true scintillator pulse distribution, while this work is aimed to be as close to the experimental conditions as possible.
The method applied in this thesis makes use of the characteristic Compton edge in the spectrum of the β-emitter Na-22 (described in more detail in Section 3.1). The amount of photons created by an electron is distributed around a given value for a certain energy. Hence detecting more photons corresponds to a larger deposited energy by the particle while detecting less photons represents a lower deposited energy. With this and the knowledge that the PDE (see Eq. (1)) is dependent on the bias voltage, it is possible to vary the amount of photons detected by changing the applied bias voltage, which can then also be seen as an artificial change in energy. This enables us to use the Na-22 spectrum with the Compton edge of Na-22, to which we are just artificially giving more or less energy by changing the PDE (compare to Fig. 7). If the deadtime is measured at the same PDE as the number of photons, a relation between the deadtime and number of photons can be obtained. Because noise (see Section 2.2.2), which can not be suppressed, contributes to the signal too, the measurements will refer to the amount of triggered pixels of the SiPM instead of the amounts of detected photons. Using this method the expected values of the PDE are ranging from 35% to 55%[3].

3.1 The Na-22 Spectrum

This section will introduce the spectrum of the radioactive isotope Na-22 which is used as a source in the following measurements. It was chosen because positrons from the β^+ decay of Na-22 annihilate with electrons, producing two 511 keV photons per e^+e^- annihilation. These photons undergo Compton scattering and give parts of their energy to electrons of which the energy distribution displays

[3]This is based on the specifications of the used SiPMs given by the manufacturer: https://www.hamamatsu.com/resources/pdf/ssd/s13360-2050ve_etc_kapd1053e.pdf

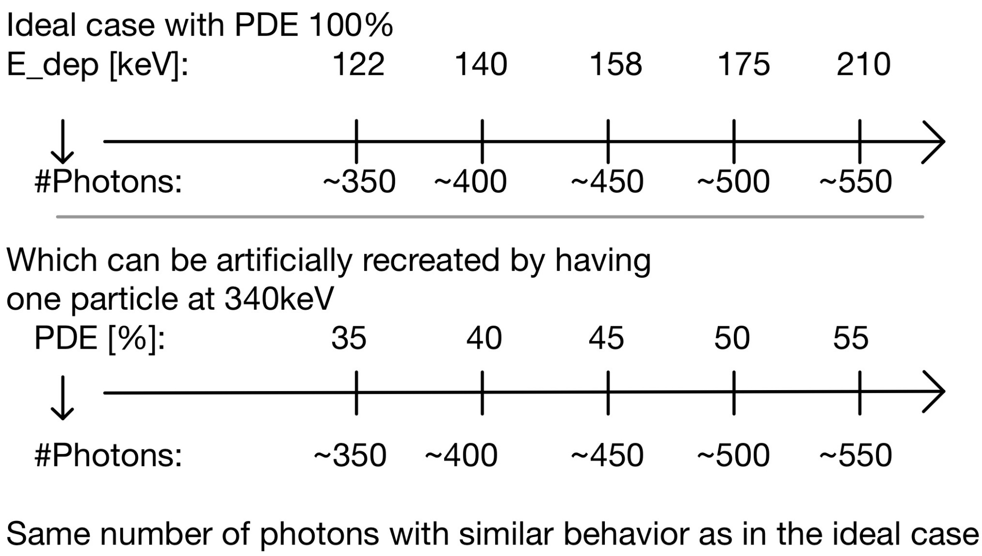

Figure 7: Sketch to illustrate the idea of comparing the case of an electron with different energies and the case of an electron at constant energy with different PDEs. The upper case shows the former while the bottom case displays the latter. The amount of photons (triggered SiPM pixels) should be similar at a constant particle energy with different bias voltages which correspond to different PDEs. The numbers are chosen based on a rough approximation from the measurements (see Section 4.4).

the Compton edge. This is a distinct feature that can be used as reference. This process will be explained in the following sections.

3.1.1 Compton Scattering and the Compton Edge

Compton scattering is a process in which a photon scatters inelastically with a free electron. The electron might be bound to an atom but the binding energy is negligible in comparison to the energy transferred from the photon. The energy transferred to the electron solely depends on the scattering angle of the photon, which has the energy E_γ. After the process, the energy of the scattered photon E'_γ can be calculated with Eq. (2) while the rest of the energy is passed onto the electron.

$$E'_\gamma = \frac{E_\gamma}{1 + \frac{E_\gamma}{m_e c^2}(1 - cos(\theta_{\gamma\gamma'}))} \tag{2}$$

Compton scattering has the highest energy transfer at a scattering angle of $\theta_{\gamma\gamma'} = 180°$ and gives thereby an upper limit for the energy transmitted to the electrons. Eq. (2) then simplifies to

$$E'_\gamma = \frac{E_\gamma}{1 + \frac{2E_\gamma}{m_e c^2}}. \tag{3}$$

As the electron energy is given by $E_\gamma - E'_\gamma$, the spectrum is expected to have a cutoff at this energy, called the Compton edge. This can be seen twice in the spectrum of the isotope Na-22 (see Fig. 8), which will be explained in detail in Section 3.1.2.

The analysis of the spectra created by the Na-22 requires a function to be fitted in the range of the Compton edge. The proposed function is based on [4]. With E_C being the energy of the Compton edge and σ being the detector resolution, it combines the behaviour of the Compton edge by using a parabolic step function (see Eq. (4)) with the detector response, which is modelled as a Gauss function, (see Eq. (5)). Those two functions are convolved into Eq. (6). The measured energy spectrum can be fitted using Eq. (6) and the point of the steepest negative slope $E_{\min}$ should approximate the value of the Compton edge. The correction factor is given by Eq. (7). $erfc(x)$ is the complementary error function.

$$r(E) = \begin{cases} aE^2 + bE + c & E \leq E_C \\ 0 & E > E_C \end{cases} \tag{4}$$

$$G(E) = \frac{1}{\sqrt{2\pi}\sigma} \exp\left[-\frac{E^2}{2\sigma^2}\right] \tag{5}$$

$$\begin{aligned} R(E) = \frac{1}{2}\left[a(E^2+\sigma^2) + bE + c\right] \cdot \operatorname{erfc}\left[\frac{E - E_C}{\sqrt{2}\sigma}\right] \\ + \left[\frac{\sigma}{\sqrt{2\pi}} a(E + E_C) + b\right] \cdot \exp\left[-\frac{(E-E_C)^2}{2\sigma^2}\right] \end{aligned} \tag{6}$$

$$E_{\min} \simeq E_C + \frac{b\sigma^2 - \sqrt{2\pi} a\sigma^3}{a(E_C^2 - \sigma^2) + bE_C + c} \tag{7}$$

3.1.2 The Na-22 Spectrum

The spectrum of Na-22 consists of four parts: two photopeaks and their corresponding Compton spectra. The first photo peak corresponds to the β^+ decay of the Na-22. Due to the low decay energy, the positron annihilates with a nearby electron creating two 511 keV photons. The spectrum to the left of the peak corresponds to the effect of photons undergoing Compton scattering with electrons before being detected. The electrons can only have a maximum energy given by Eq. (3). The same happens at 1275 keV, where the photons result from the decay of excited Ne-22 which is a β^+ decay product of Na-22. The spectrum in Fig. 8 shows the energy distribution of the photons with their distinct peaks and after their Compton scattering. The Compton edge given by Eq. (3) is expected to be sharp but is smeared out as a consequence of the detector resolution.

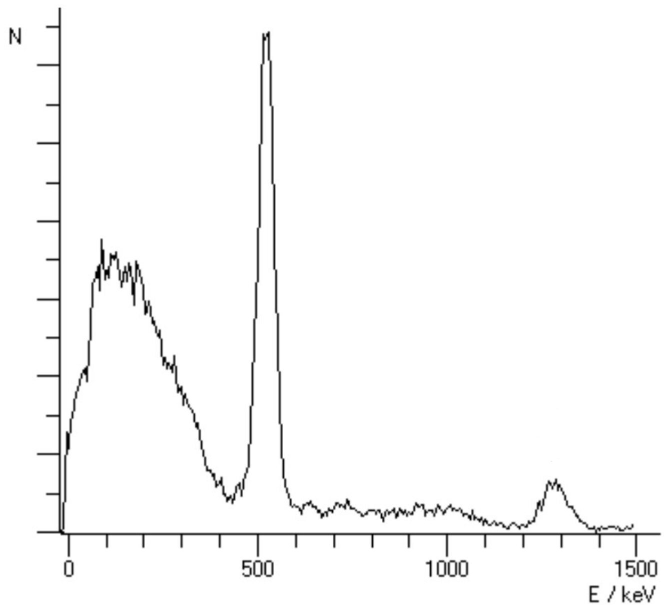

Figure 8: Na-22 spectrum [5] where the two photopeaks and Compton edges are visible.

3.2 Measurement Setup

The measurements presented in this thesis consist of three major sets: Firstly, the deadtime of the MuTRiG chip is measured using the Na-22 source. As a next step, the heights of the SiPM signals produced by the Na-22 source are measured for different bias voltages. These signal heights will later be calibrated to the amount of SiPMs which were triggered. The amount of pixels triggered is a reference to the amount of photons detected. The calibration measurement is the third measurement, in which the signal heights of single pixels will be determined.
All the measurement setups are placed inside an environment at a constant temperature of 10 °C, while for each measurement the same SiPM matrix board is used. There are 16 SiPMs with scintillators assembled on the board which distributes the bias voltage to the SiPMs and transmits their signals. This matrix board is connected via a flexprint to a transition board which is fitted with an input for the bias voltage and a 16-channel connector (see Fig. 9). For all the measurements, the same bias voltage is set inside the range of 53 V to 59 V with a step size of 0.5 V. The lower voltage limit is given by the breakdown voltage of the SiPMs at approximately 52 V (compare to Table 1 for the exact values) while the upper limit is given by the maximum thresholds which can be set with MuTRiG to filter out noise. The transition board is connected either to a custom-designed printed circuit board hosting the MuTRiG (for the deadtime measurement), or to another adapter printed circuit board which allows for the direct read-out of the SiPM signals (for the calibration and the signal heights measurements). Those

boards are connected to an oscilloscope[4] for the readout.
The applied bias voltage on the SiPM is influenced by the MuTRiG and shifted by a constant to a lower value which needs to be considered. All set bias voltages in the following sections are labelled in the value which was set in the deadtime measurement. Hence during the signal heights and calibration measurements the set voltage was adapted to be the same true value as in the deadtime measurement. For this the values V_{shift} (listed in Table 1) are determined by using a printed circuit board without SiPMs (called blind matrix shown in Fig. 25 in the Appendix). This is done by connecting a voltmeter at the connectors where the bias voltage is applied to the SiPMs. By comparing the set values V_{set} to the measured values, it is visible that the true bias voltage with the MuTRiG chip used to measure is given by $V_{\text{set}} - V_{\text{shift}}$.

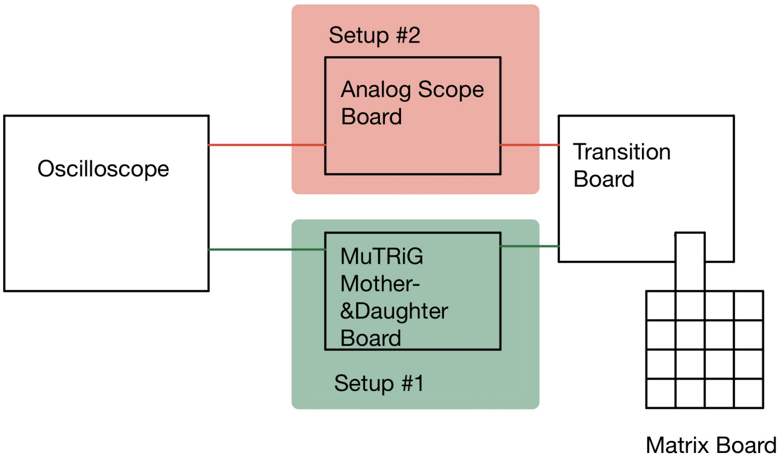

Figure 9: Sketch of the measurement Setups. The green box represents the deadtime measurements while the red box represents the signal heights and calibration measurements. Images of the parts are shown in the appendix.

3.2.1 Deadtime Measurements

In this part of the experiment, the goal is to measure the distribution of the deadtime for each of the 16 channels in the matrix, which is read out with the MuTRiG. The Na-22 radiation source is placed on top of the tile matrix. The MuTRiG is hosted on a daughterboard/motherboard combination, which was designed specifically for laboratory measurements. The daughterboard with the assembled MuTRiG is connected to the transition board of the matrix, as well as to the motherboard. The motherboard allows the monitoring of the digital output of a MuTRiG channel using e.g. differential probes and the oscilloscope. This feature is used to observe the time that the MuTRiG detects a signal above the timing threshold as shown in Fig. 6 which corresponds to the time a channel is not able

[4] Teledyn LeCroy SDA 840 Zi

to detect a new particle. This information is then read out with the oscilloscope and stored for later analysis. The timing threshold is chosen such that the timing threshold of each channel is as low as possible and above electronic noise level. The energy trigger is chosen to filter out most of the dark count rate. The energy trigger thereby requires the signal to have a minimum energy while the timing trigger is supposed to measure the full length of a signal.

3.2.2 Signal Height Measurements

This section is dedicated to measuring the distribution of amplitudes of the SiPM signals generated by the Na-22 source. The SiPMs are read out directly with the oscilloscope via the Analog Scope Board (which is a custom-made board for direct single channel readout of the SiPMs). In this case, as mentioned in Section 3.2, the bias voltages were set to be the same as the ones when the MuTRiG was used to measure. For the measurements, the Na-22 source is placed on top of the tile matrix again and the signal height for each pulse signal is measured and stored.

3.2.3 Calibration Measurements

A calibration of the signal height measurement can be done by looking at low photon levels at the SPS. Low photon levels refers to processes in which only one up to around ten photons are detected. For those processes, the amplitudes of the SiPM signals are measured and saved in a histogram resulting in a SPS. In this SPS, peaks can be observed which correspond to different amounts of triggered pixels and from their position a relation between charge and detected photons can be obtained. The noise from Section 2.2.2 has a signal level in the order of low photon levels triggering around one to three pixels, but more triggered pixels are needed for better statistics. In this case a laser has been used instead of a radiation source. It was set, to emit only a few photons, that reach the SiPM, creating signals at low photon levels with amplitudes resulting from only one to ten photons hitting the SiPMs. Due to the photons having a low energy the scintillating material was not excited. Contrary to the argument that a pulsed light source has a different emission of light than scintillation light has for normal signals, it makes no difference in this case with low photon numbers since the photons hit the SiPM almost at the same time.
The SPS are obtained by directly reading out the SiPM signals with the previously mentioned Analog Scope Board with separate SMA connectors for each channel. The bias voltage is adapted as in the previous subsection to match the voltages from the deadtime measurements. The signals were amplified by 50 because of their low amplitude and the factor is considered afterwards in the analysis.

4 Results

This chapter displays the methods used to analyse the data as well as the results. The analysis of the three data sets is ordered as in Section 3.2, while in Section 4.4 the combined result are presented. In Section 4.5 the results are used to make an estimate of how the deadtime behaves for 1 MeV deposited by electrons and Section 4.6 contains a short discussion of the results.
In the following sections the channels and tiles are numbered from 16 to 31 with two channels (24 and 30) being excluded from the measurements. The data from channel 24 is not used due to a connection issue between the transition and the analog scope board, which lead to a signal distortion during the signal height measurement. This could not be investigated further within the limited time of this thesis. Channel 30 was not used in the measurements because during the deadtime measurements the MuTRiG channel showed a too large noise overlapping with the signal.
In this section the bias voltages are again given as they were set for the MuTRiG, as explained in Section 3.2. The voltage shift induced by the MuTRiG, as well as the breakdown voltages determined from the calibration measurements, are listed in Table 1.

Ch Number	$V_{\mathrm{Br}}[V]$	$V_{\mathrm{shift}}[V]$
16	52.132 ± 0.005	0.589
17	51.704 ± 0.011	0.633
18	51.736 ± 0.008	0.603
19	52.035 ± 0.009	0.633
20	51.663 ± 0.010	0.628
21	51.875 ± 0.010	0.633
22	51.940 ± 0.013	0.633
23	51.758 ± 0.011	0.545
25	51.738 ± 0.006	0.538
26	51.929 ± 0.011	0.614
27	51.731 ± 0.005	0.538
28	51.737 ± 0.008	0.538
29	51.642 ± 0.014	0.651
31	51.712 ± 0.008	0.538

Table 1: Reference table for the SiPM channels. The breakdown voltage is measured during the calibration measurement.

4.1 Deadtime Measurements

In order to identify the Compton edge Eq. (6) is fitted to the data. The fits converge despite the fact that the deadtime and not the energy is plotted on the x axis. The fits are susceptible to changes of the fitting boundaries and have very large $\chi^2_{/red}$ values, hence the fits errors are probably given underestimated. This will be considered in Section 4.5 in which the error will be estimated. In all cases the parameter E_C (in units of deadtime) does not represent the Compton edge. It is always shifted too far to the left into the plateau and the calculated value from Eq. (7) shows a false position for the maximum gradient. This might be based on the fact that the detector is targeted to have a high timing resolution while the energy resolution is not of importance. This results in the mathematical description of Section 3.1.1 not being applicable because the theory, that the detector resolution is given by a Gaussian function is not accurate. Still, with the motivation, that the Compton edge is near the position of maximum negative slope, given in [4] the point of maximum negative slope was chosen as the distinct point of the spectrum (from now on, it will be referenced just as maximum slope). It is sufficient for the thesis, because solely a distinct point is needed to map the deadtime and the height measurements as long as it appears in both measurements. To determine the error of the position of the maximum slope, the function parameters are varied by their error and the position of the slope for the varied graphs is calculated. The difference between the initial position and the positions that arises from varying the parameters gives a value of the uncertainty. An example of a measured deadtime spectrum is shown in Fig. 10, while its behaviour at different bias voltages can be seen in Fig. 11 for channel 20.

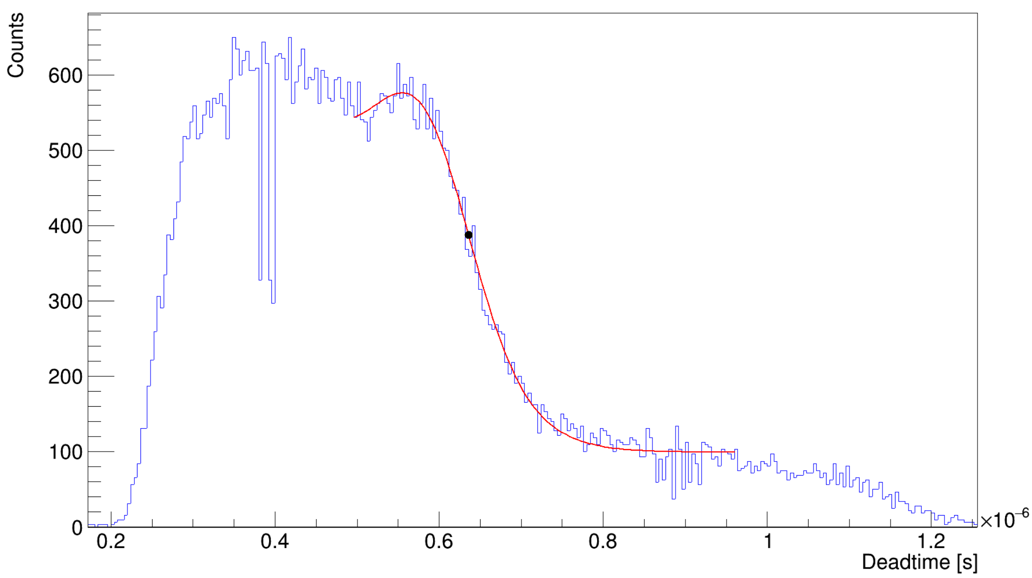

Figure 10: Measured deadtime spectrum of the Na-22 source for channel 20 at a set voltage of 57 V. The rise for values below 500 ns corresponds to noise. The red line shows the fit and the black dot indicates the point of the maximum gradient. Some bins in the area of 400 ns and 900 ns have less counts due to binning effects in the oscilloscope.

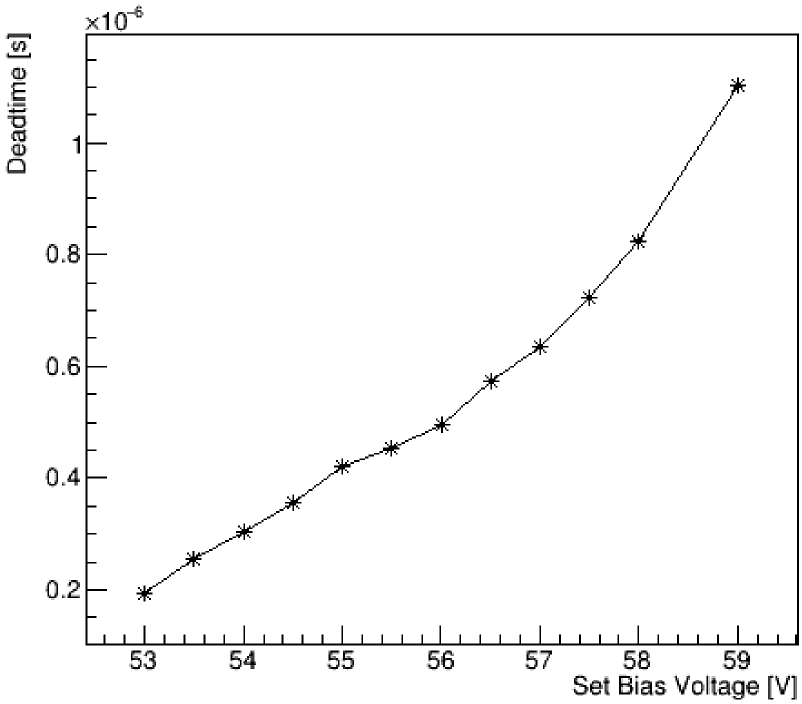

Figure 11: Deadtime of channel 20 at the point of the maximum gradient close to the Compton edge in the Na-22 spectrum for different bias voltages.

4.2 Signal Height Measurements

The data of the signal height measurements is analysed as described above for the deadtime measurements. A notable difference in the spectra is the increased noise due to the signal not being filtered by the MuTRiG chip, making the fit more challenging. Fig. 12 displays a fit to the spectrum for channel 20 at a bias voltage of 57 V. The black dot indicates the position of the maximum slope with small errors which are again probably underestimated by the fit due to the high $\chi^2_{/red}$ values. This will be considered in Section 4.5 in which the error will be estimated. Fig. 13 displays the behaviour of the maximum slope for different bias voltages.

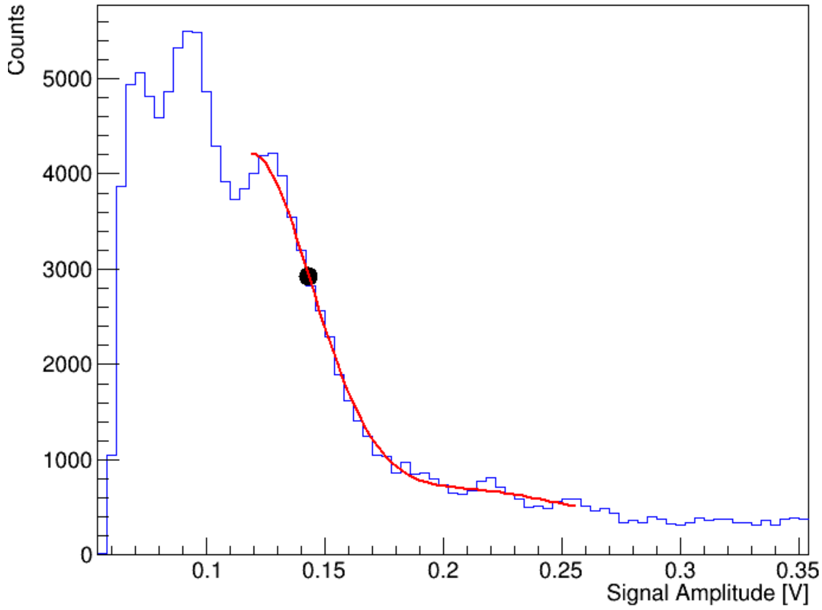

Figure 12: Measured peak height spectrum with the Na-22 source of channel 20 at a set value (corrected for the MuTRiG shift) of 57 V. The red line shows the fit and the black dot indicates the point of the maximum gradient. The peaks lying on the Compton plateau at 0.04 V and 0.08 V correspond to noise.

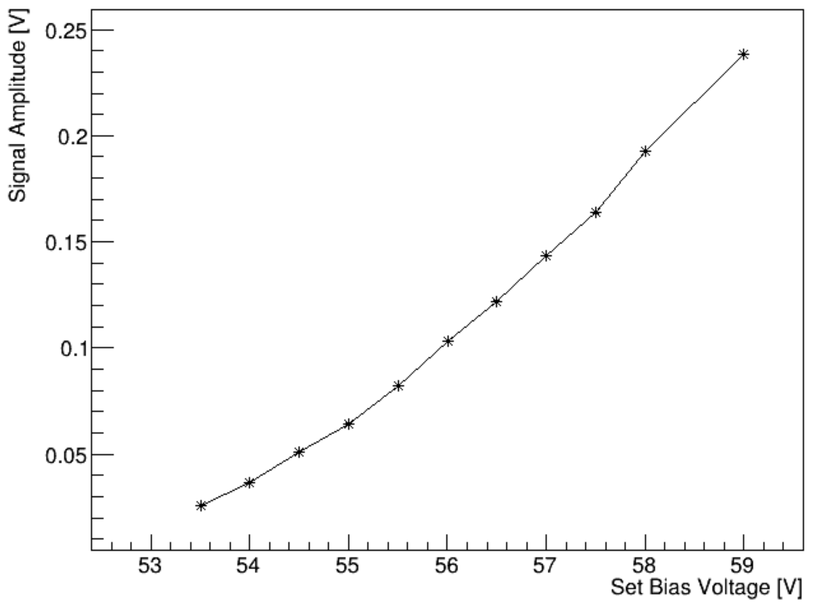

Figure 13: Signal height at the point of the maximum gradient close to the Compton edge in the Na-22 spectrum for different bias voltages.

4.3 Calibration Measurements

The analysis of the single photon spectra are done for each channel and voltage by fitting a Multi-Gauss function to a selection of peaks to obtain their position. All peaks with a minimum height of 30% of the highest peak are fitted. The peak positions are then numbered by the amount of triggered pixels and the numbers are plotted against the corresponding positions. The ratio of signal height to number of triggered pixels is obtained by fitting a linear function. This will be used to identify the number of triggered pixels for the slope positions which are given in the unit of signal height from the previous section. Figs. 14 and 15 display an example SPS and the fit to obtain the calibration value. The resulting values are divided by a factor 50 for further analysis because of the amplifier used.
The measurements of the SPS at different voltages enables the acquisition of the breakdown voltage of each channel. To get this value, the gain (the slope of the fit to the peak positions) is plotted for each set bias voltage and a linear function is fitted. Fig. 16 displays this for channel 20. The breakdown voltage is then the zero crossing of the linear function. The determined breakdown voltages are listed in Table 1.

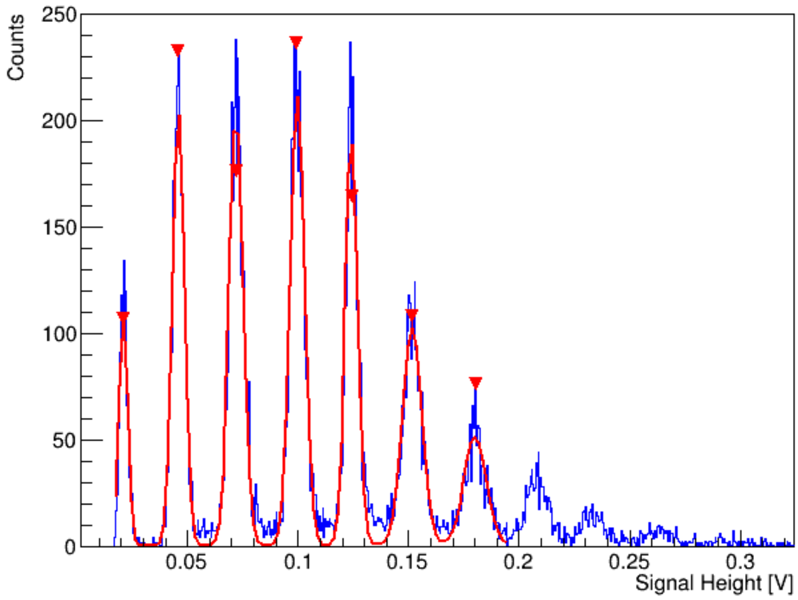

Figure 14: The graph shows the SPS of channel 20 taken at bias voltage of 57 V, with a Multi-Gaussian being fitted to a selection of peaks. The signal height values need to be divided by a factor of 50 because of the amplifier used.

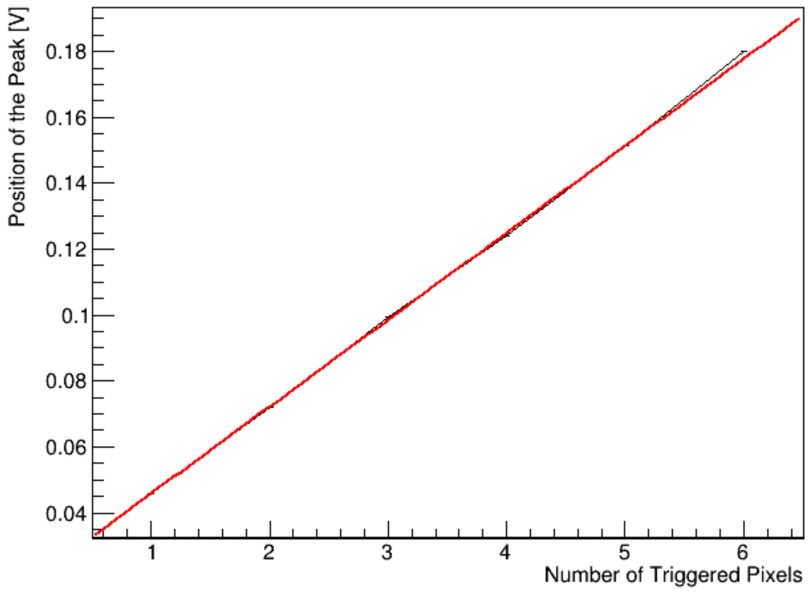

Figure 15: The Figure shows the linear fit to the peak positions. The signal height values need to be divided by a factor of 50 because of the amplifier used.

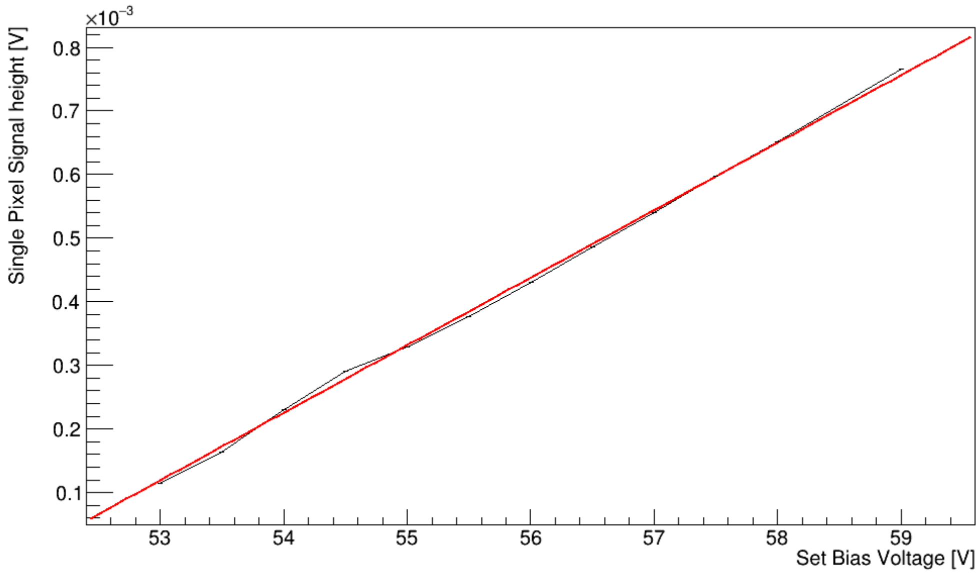

Figure 16: Single pixel signal height at the point of the maximum gradient close to the Compton edge in the Na-22 spectrum for different bias voltages.

4.4 Combined Results of the Measurements

The final steps are to combine the results to obtain the final relation between the amount of triggered pixels and the deadtime. The graphs of the deadtime and the signal heights at maximum slopes at different voltages are merged into a single graph. This is done by matching the deadtime to the signal height at the same bias voltage. This is displayed in Fig. 17 for channel 20, where the deadtime is

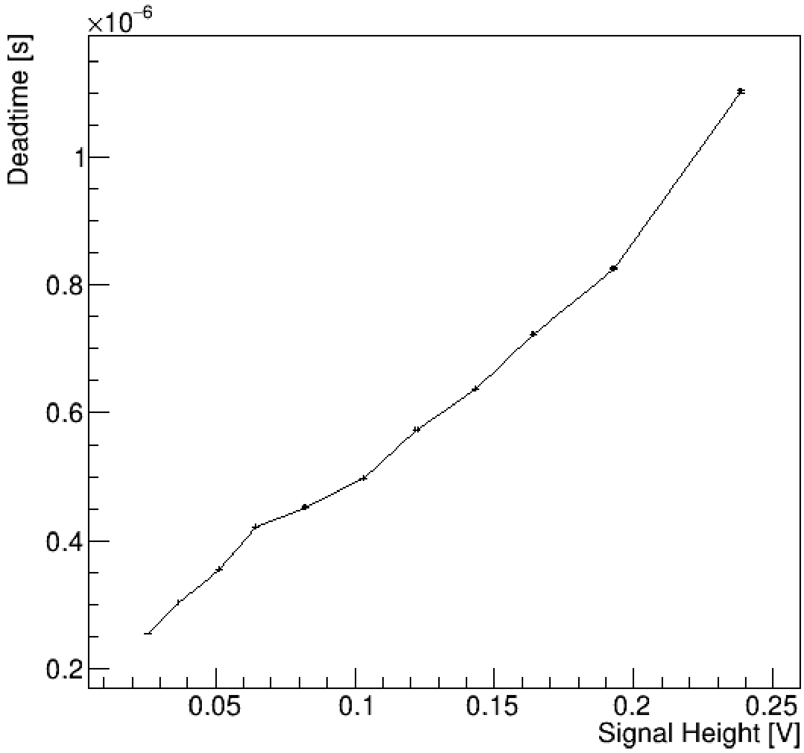

Figure 17: Deadtime depending on signal height for channel 20.

given for different signal heights. This shows that for every measured bias voltage at the lowest time trigger threshold for the energy around the Compton edge at 340.6 keV, the deadtime is above the previously assumed amount of up to 260 ns [1] (with the electrons energy at the Compton edge being calculated by E_γ-$E_{\gamma'}$ from Eq. (3) with $E_\gamma = 511\,\text{keV}$).
In order to convert the values for the x axis in Fig. 17 to the unit of pixels triggered, the data points are divided by their corresponding gain at the given bias voltage. Fig. 18 displays the result for channel 20 and Fig. 19 shows the results for all channels. The strong increase at high numbers of pixels is due to the fact that the gain per pixel also increases the deadtime. This increase amplifies the deadtime increase with the amount of triggered pixels. Additionally, noise sources which increase with the bias voltage but do not contribute to the signal height can also add to the steeper rise of the deadtime on the right side of Fig. 17. All three noise sources listed in Section 2.2.2 increase with the bias voltage. While dark count rate and afterpulses do not necessarily contribute to the signal height they still are able to increase the time over threshold and thereby the deadtime. This happens if the noise creates signals direct before the real signal pulse or during its decay.

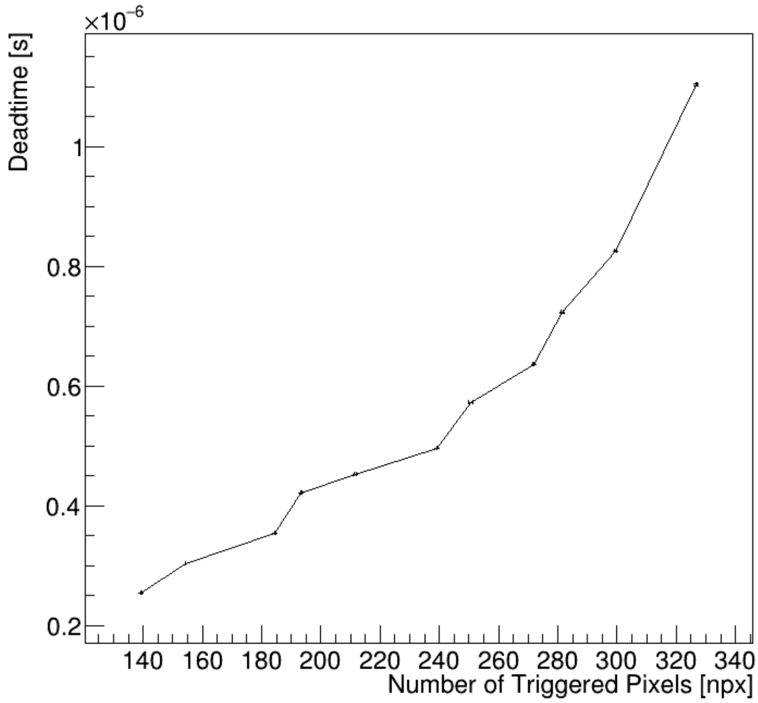

Figure 18: Deadtime depending on triggered pixels for channel 20. The strong increase to higher photon number comes from an increase in gain as well as an increase in noise.

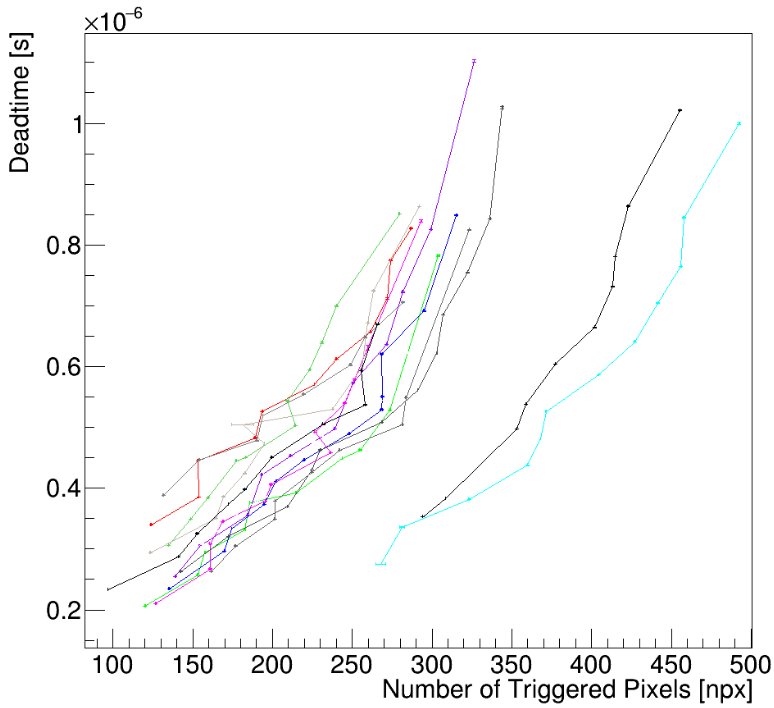

Figure 19: Deadtime depending on number of triggered pixels for all measured channels. On the right the two channels which are out of place are channel 16 (black line) and channel 22 (cyan).

4.5 Estimations for the Mu3e Experiment

In order to make predictions on the behaviour of the deadtime in Mu3e experiment like conditions an error, which is not clearly underestimated, is needed. Therefore, an estimation of the errors of the three measurements will be done here. The maximum uncertainty on the position of maximum slope in the deadtime and signal height measurements can be estimated by assuming that it should be in the area of slope between the constant plateaus. Looking at Figs. 10 and 12 and other channels and bias voltages this corresponds to roughly 10% relative uncertainty for the deadtime measurements and 15% for the signal height measurements. The error on the calibration measurement determining the gain is estimated to be up to 1% and hence in the error propagation negligible because it is far lower than the other values. These estimated errors are propagated through the analysis and will be included in the calculations and Figs. 20 and 22. For the later determination of the deadtime for a given number of triggered pixels a linear function is fitted to the data. The linear function was compared to other polynomial functions of the second and third degree and to an exponential function as well. Due to the fact that there is no model for this relation, the functions were chosen to model an increasing behaviour to give an estimate on the upper limits of the deadtime. The linear function was deemed most suitable to describe the data.

To account for the fact that the single pixel gain and thereby the deadtime per single pixel increases, the signal height values are normalised to the gain at a single chosen bias voltage. Hence the x axis shows a relative signal which corresponds to the number of pixels triggered at the given signal heights for the chosen bias voltage. Fig. 20 displays the relative signal in number of triggered pixels which are referenced to the bias voltage of 54 V. The behaviour of all channels referenced to 54 V is shown in Fig. 21. Fig. 22 shows the relative signal referenced to a higher bias voltage at 57.5 V. In this case the signal heights corresponds due to the higher gain to less pixels firing while the deadtime still stays at its value.

If we consider that the scintillating material is polyvinyltoluene with a density of $1.023\,\frac{\mathrm{g}}{\mathrm{cm}^3}$ and using the NIST [6] data from Fig. 23 we can make some estimates. Electrons with an energy around 341 keV, i.e. the energy of the Compton edge, loose more than 1 MeV per centimetre. Thereby they deposit all their energy in the scintillating material which has the dimension of $6.3 \times 6.21 \times 5.0\ \mathrm{mm}^3$. The data sheet [7] of the scintillating material states that approximately 10200 photons per MeV are expected. For the energy at the Compton edge of 341 keV, this corresponds to approximately 3468 photons being produced. The true amount of triggered pixels in dependence of the deadtime can be calculated by dividing the signal heights (shown in the case of channel 20 for Fig. 13) by the gain values

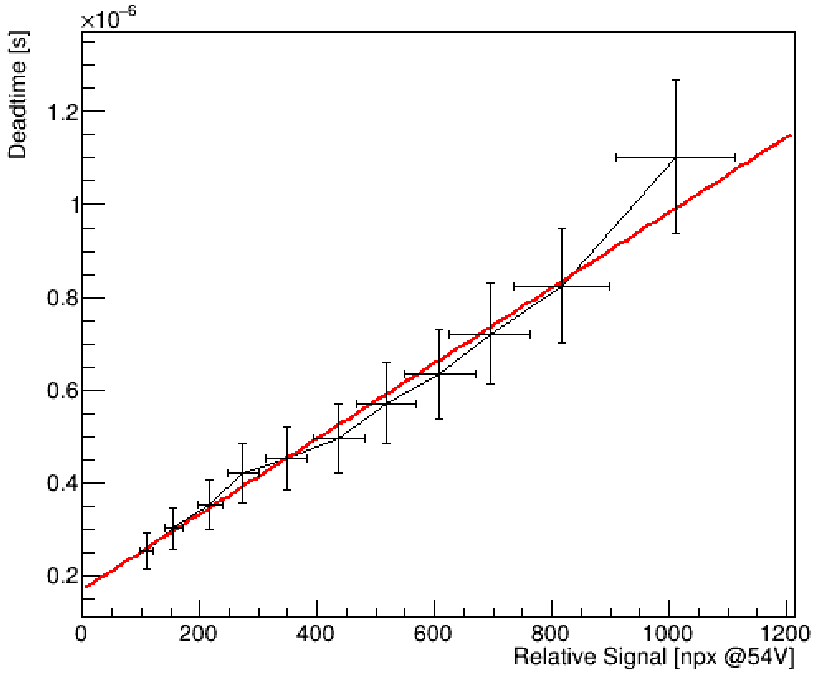

Figure 20: Deadtime depending on the relative signal normalised to the set bias voltage of 54V for channel 20. The errors are originating from the error estimation and the linear fit function is drawn in red.

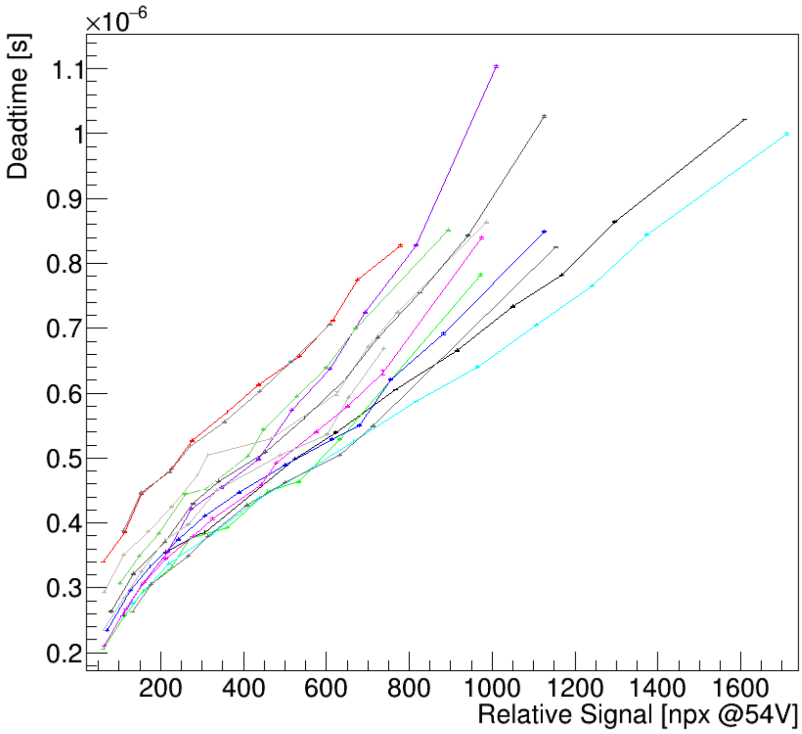

Figure 21: Deadtime depending on the relative signal of fired pixels normalised to the set bias voltage of 54V for all channels.

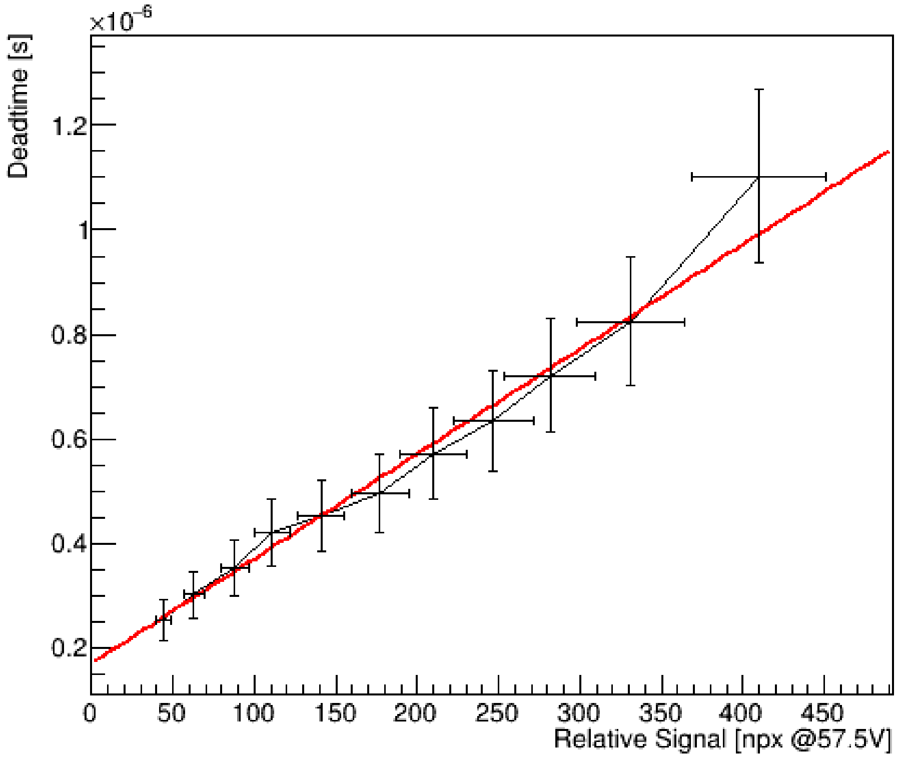

Figure 22: Deadtime depending on relative signal normalised to the set bias voltage of 57.5V for channel 20. The errors are originating from the error estimation and the linear fit function is drawn in red.

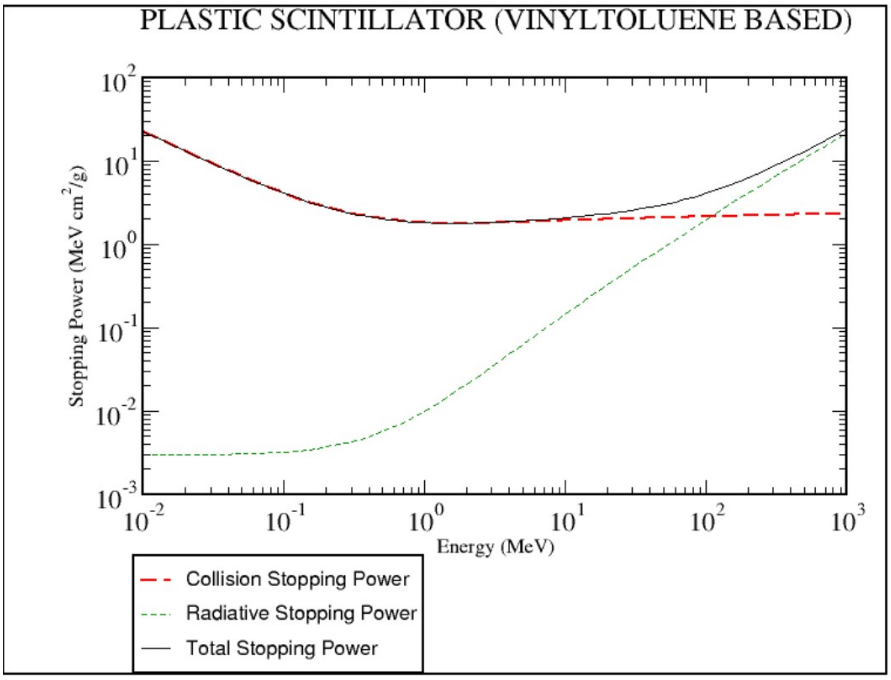

Figure 23: Stopping power for electrons in a polyvinyltoluene based scintillating material. [6]

(shown in the case of channel 20 for Fig. 16) for the respective bias voltage. Fig. 24 shows which amounts of triggered pixels really were measured for channel 20 at different bias voltages. Given the expected number of photons of 3468, this shows

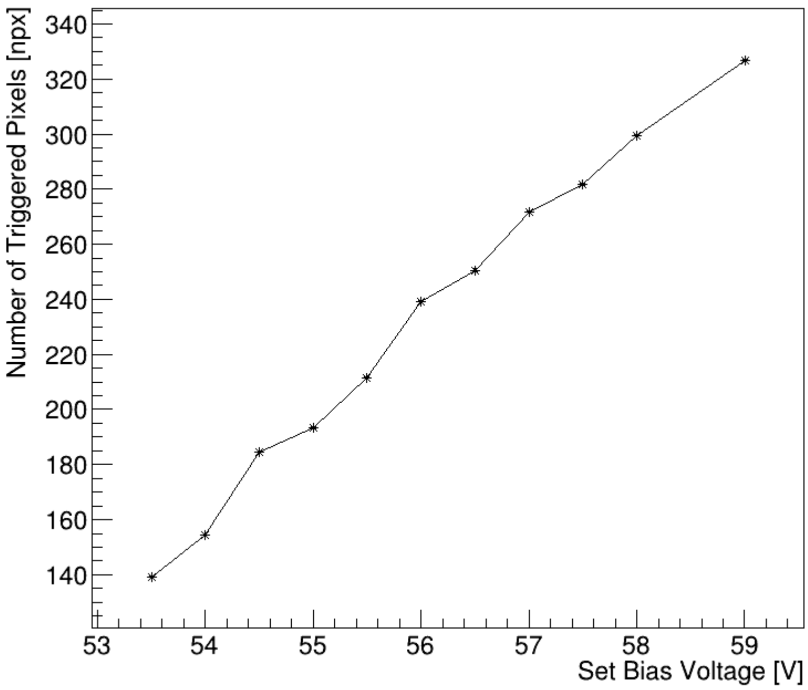

Figure 24: Measured amount of triggered pixels for the point of maximum slope at different bias voltages for channel 20.

that we measured approximately 140 to 320 triggering pixels at different voltages. This corresponds to a percentage of 4% to 10% of the amount of produced photons resulting in pixels triggering for the different bias voltages. At a bias voltage of 54 V this means that including noise the photons cause approximately 5% of the amount of generated photons in pixels triggering due to noise and photons. This does not exactly represent the PDE because there is also loss due to photons leaving the scintillating material on the edges, hence not arriving at the SiPM. Considering that the average deposited energy in a tile is 1 MeV in the Mu3e experiment [1], we expect around 10200 photons to be produced, thus corresponding to about 510 pixels firing at a bias voltage of 54 V. Since the data of channel 20 normalised to 54 V covers the range of up to 1000 triggered pixels, the deadtime of 510 pixels can be extracted from the fit to Fig. 20 to be around (0.59 ± 0.06)µs. The signal loss ϵ is then calculated using the the deadtime τ and an expected rate of $n = 60$ kHz, by [8]:

$$\epsilon = 1 - e^{-n\tau}. \tag{8}$$

This would result in signal loss of $(3.5 \pm 0.3)\%$ for a deadtime of (0.59 ± 0.06)µs. If the same calculation is done for a bias voltage of 57.5 V, we have around 8% of the original amounts of photons in triggering pixels. This means about 812 pixels are triggered which is twice the maximum value covered in Fig. 22. Extrapolation, using a linear function as previously mentioned, yields a deadtime of (1.8 ± 0.22)µs which would correspond under the current assumptions to a signal loss of up to $(10.2 \pm 1.1)\%$.

4.6 Discussion and Limits of the Method and the Predictions

The errors of the positions of the slope in Sections 4.1 and 4.2 are very small which, as discussed before in Section 4.1, probably originate from underestimating the fit errors due to the complicated model of the data. Thus, the method fitting a Compton edge is not recommended because producing a good with appropriate errors is difficult. Those errors are passed on through the analysis and are combined with the errors from Section 4.3, which has low errors too but better fits with a lower χ^2_{red} which does not add additional uncertainty during the error propagation. The trend of the increasing deadtime behaviour along the measured range still seems fitting if we compare all the channels in Figs. 19 and 21 hence in Section 4.5 the own error estimation with the increasing behaviour seems justified. While the linear function was the best fit for the data range with continuously increasing behaviour it is probable, that the analysis over a wider range of data shows a different and not so strongly increasing behaviour because with the increasing bias voltage also increasing noise effects where measured.

The method of altering the bias voltage to induce a change solely on the PDE should also be handled carefully because as visible in Section 4.4 the single pixel gain has a strong effect on the deadtime too.

Finally, the estimations for signal loss rates are only able to give a rough approximation of the upper limit of the maximum deadtime of a single channel. Inside the real Mu3e experiment, effects such as the settings of the timing thresholds, which has not been varied, have additional effects to the signal loss enabling additional optimisation of the deadtime. Testbeams showed too, that a lower bias voltage at 54 V still maintains a timing resolution well below 100 ps.

5 Summary

The Tile Detector aims to provide a high timing resolution at high detection rates for the Mu3e experiment which searches for the Lepton-Flavor violating decay $\mu^+ \rightarrow e^+e^+e^-$. Previous tests and optimisations focused on the time resolution of the Tile Detector. Therefore this work was aimed to make a first quantitative assessment of the capability of the Tile Detectors components to maintain a high detection efficiency at high rates of up to 60 kHz. To achieve this, the goal was to measure the behaviour on how the deadtime of a single channel is influenced by the energy deposited by electrons inside the detector. The deadtime of a single channel was defined as the time where the MuTRiG chip is processing the signal and the arrival information of a new incoming signal cannot be measured.
The usual approach to measure this relation between deadtime and deposited energy would be to take the test setup to a particle accelerator. Due to restrictions this was not possible. Because the detector is made for electron detection, an approach with high energy photon sources where the energies are known was not possible either. Therefore, a different approach was taken with the radiation source Na-22. In the end, resulting from a chain of events, electrons from Compton scattering are detectable with a maximum energy of 341 keV at the Compton edge. The idea behind the measurements was to change the perceived energy by changing the detecting SiPM parameters. This was done by changing the bias voltage applied to the SiPMs and thereby changing the photon detection efficiency. The photon detection efficiency describes the probability that a photon entering a SiPM leads to an electrical signal. To change the photon detection efficiency has a similar effect like the change of the deposited energy and thus the amount of scintillation light produced.
The deadtime was measured for the Na-22 spectrum as well as the signals heights created. For those measurements the approximate position of the Compton edge was identified at different bias voltages. This already showed that the deadtimes are higher than the values of about 260 ns [1] which were previously anticipated. With the aid of a calibration measurement which determined the gain of the SiPMs at different bias voltages the number of triggered pixels was calculated. This also showed, that the gain itself with its dependence on the bias voltage has a strong influence on the deadtime. With this accounted for, the relation of the deadtime to the relative signal was calculated. This relative signal gives an approximation about the number of triggered pixels at a given bias voltage. Based on those results an estimation on the signal loss of a single channel in Mu3e like conditions was performed. The estimation assumed an average energy deposition of 1 MeV. It concludes, that for a bias voltage of 54 V a deadtime of (0.59 ± 0.06)µs can be

expected and this would mean a signal loss of up to $(3.5 \pm 0.3)\%$. A strong increase of the signal loss is given for higher bias voltages, for example at 57.5 V with an estimated deadtime of (1.8 ± 0.22)µs which would mean a loss of $(10.2 \pm 1.1)\%$. Those results show, that it is important to include the deadtime in the next optimisation measurements because the signal acquisition is influenced by it. Additionally the influence of adjusting the timing thresholds should be investigated.

A Images of the Electronics

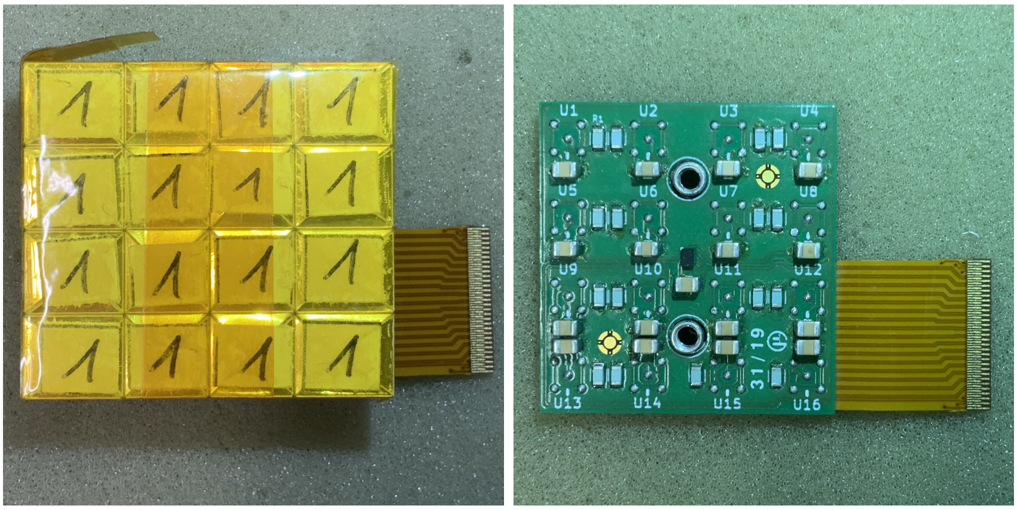

Figure 25: on the left hand side is the used matrix board while on the right hand side a matrix board without SiPMs and scintillating tiles is displayed. It was used to measure the MuTRiG bias voltage offset.

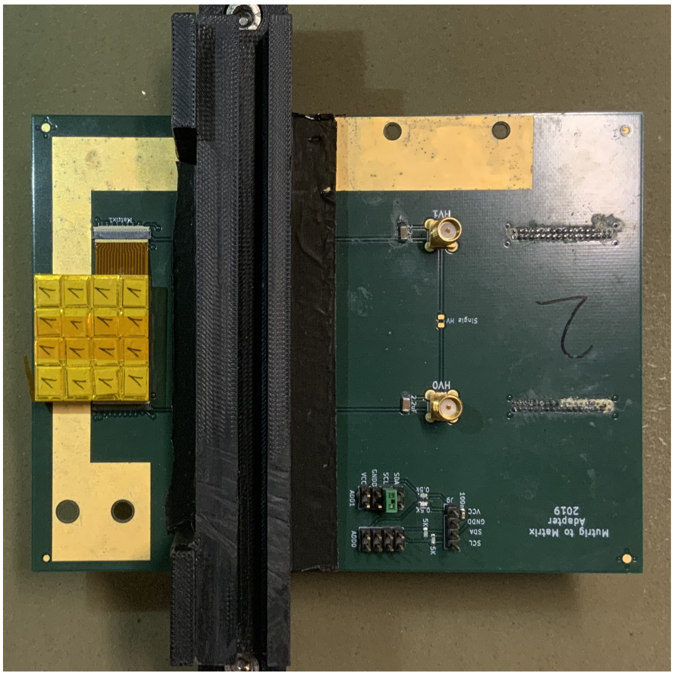

Figure 26: Transition board with the matrix on top.

A.1 Setup 1

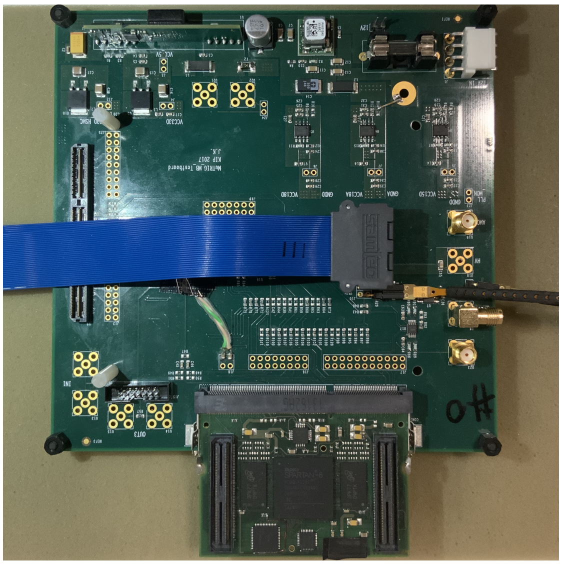

Figure 27: Motherboard with an FPGA connected at the bottom.

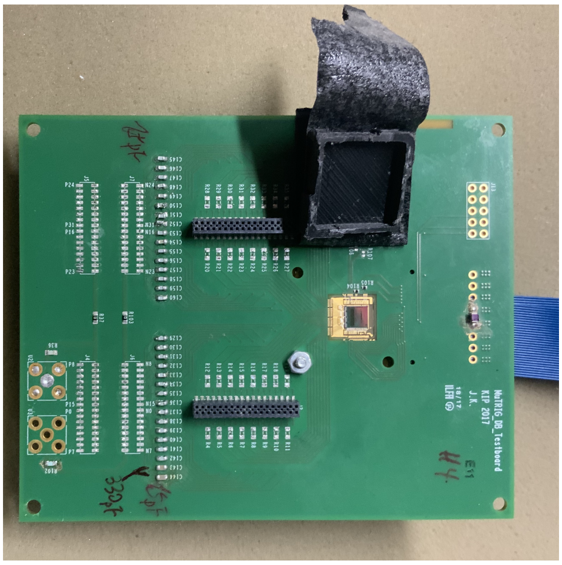

Figure 28: Daugtherboard with the MuTRiG.

A.2 Setup 2

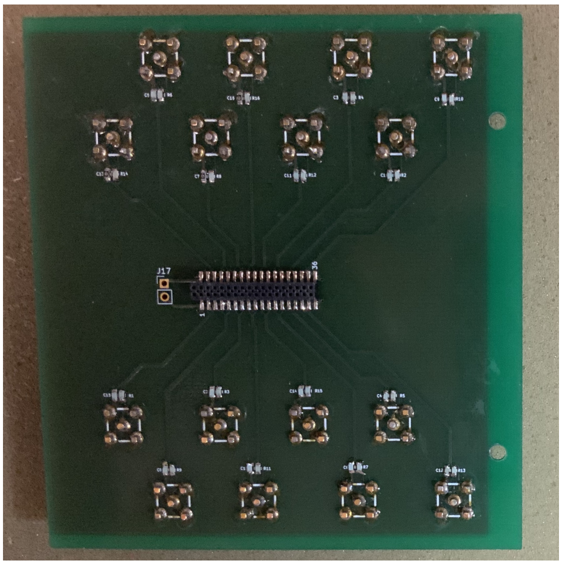

Figure 29: Upper side of the Analog Scope Board.

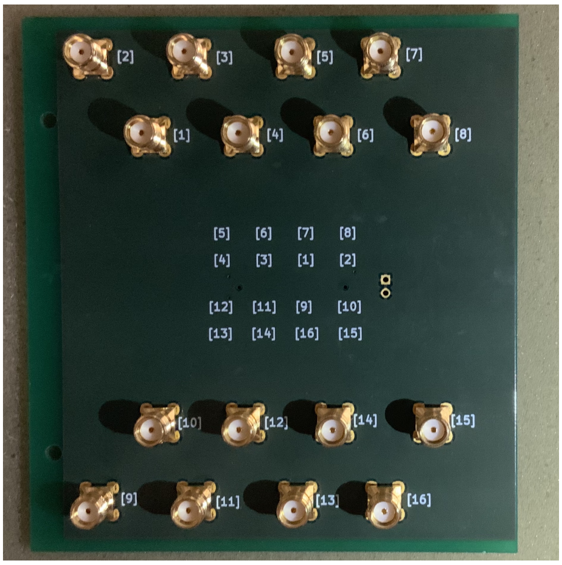

Figure 30: Bottom side of the Analog Scope Board with the SMA connectors for the oscilloscope readout.

References

[1] P. Eckert, *The Mu3e Tile Detector*. PhD thesis, Universität Heidelberg, 2015.

[2] A. Blondel *et al.*, "Letter of Intent for an Experiment to Search for the Decay $\mu \rightarrow eee$," 2012.

[3] H. Chen, *A Silicon Photomultiplier Readout ASIC for the Mu3e Experiment*. PhD thesis, Universität Heidelberg, 2018.

[4] M. J. Safari, F. A. Davani, and H. Afarideh, "Differentiation method for localization of compton edge in organic scintillation detectors," 2016.

[5] LD-Didactic, "Natrium-22." `https://www.ld-didactic.de/software/524221de/Content/Appendix/Na22.htm`. [Online; accessed 4-September-2020].

[6] M. A. Z. Martin j. Berger, J S. Coursey, "ESTAR, PSTAR and ASTAR: Computer Program for Calculating Stopping-Power and Range Tables for Electrons, Protons, and Helium Ions(Version 1.21)." `http://physics.nist.gov/Star`, January 1999.

[7] E. TECHNOLOGY, "Data Sheet EJ-228." `https://eljentechnology.com/products/plastic-scintillators/ej-228-ej-230`. [Online; accessed 4-September-2020].

[8] C. Graf, "A calibration scheme for the mu3e tile detector," masterarbeit, Universität Heidelberg, March 2015.

[9] A. Blondel *et al.*, "Research Proposal for an Experiment to Search for the Decay $\mu \rightarrow eee$," 2013.

[10] J. Bleck-Neuhaus, *Elementare Teilchen*. SpringerLink : Bücher, Berlin, Heidelberg: Springer Berlin Heidelberg, 2010.

Acknowledgements

At this point I want to thank everyone who accompanied me through my Bachelor studies and supported me throughout the process of writing my Bachelor thesis.

I am thankful that Prof. Dr. Schultz-Coulon gave me the opportunity to write my thesis inside his group and for his support. I also thank apl. Prof. Dr. Yuri Litvinov for being the second examiner.

Thanks to the whole group for taking me in and always having some time to answer my questions.

I am especially thankful to Hannah Klingenmeyer for her constant support and thorough proof reading my thesis. Additionally, I want to thank Dr. Rainer Stamen and Falk Bartels for their support of my thesis too.

Finally I want to thank my family and friends for their help and always productive discussions.

Erklärung

Ich versichere, dass ich diese Arbeit selbstständig verfasst und keine anderen als die angegebenen Quellen und Hilfsmittel benutzt habe.

Heidelberg, den 6. September 2020,